catalysts

MDPI

Article

Novel Synthesis of Plasmonic Ag/AgCl@TiO_2 Continues Fibers with Enhanced Broadband Photocatalytic Performance

Nan Bao [1,*], Xinhan Miao [1], Xinde Hu [1], Qingzhe Zhang [2], Xiuyan Jie [1] and Xiyue Zheng [1]

[1] Shandong Key Laboratory of Water Pollution Control and Source Reuse, School of Environmental Science and Engineering, Shandong University, Jinan 250100, China; miaoxh1991@outlook.com (X.M.); hxd7887@163.com (X.H.); jxiuyan0413@163.com (X.J.); zhengxiyue1995@163.com (X.Z.)

[2] Institut National de la Recherche Scientifique (INRS), Centre Énergie Materiaux et Télécommunications, Université du Québec, 1650 Boulevard Lionel-Boulet, Varennes, Québec, QC J3X 1S2, Canada; zhangqingzhe17@163.com

* Correspondence: baonan@sdu.edu.cn; Tel.: +86-531-8836-4724

Academic Editors: Vladimiro Dal Santo and Alberto Naldoni
Received: 28 February 2017; Accepted: 13 April 2017; Published: 17 April 2017

Abstract: The plasmonic Ag/AgCl@TiO_2 fiber (S-CTF) photocatalyst was synthesized by a two-step approach, including the sol-gel and force spinning method for the preparation of TiO_2 fibers (TF), and the impregnation-precipitation-photoreduction strategy for the deposition of Ag/AgCl onto the fibers. NaOH aqueous solution was utilized to hydrolyze $TiCl_4$, to synthesize TF and remove the byproduct HCl, and the produced NaCl was recycled for the formation and deposition of Ag/AgCl. The surface morphology, specific surface area, textural properties, crystal structure, elemental compositions and optical absorption of S-CTF were characterized by a series of instruments. These results revealed that the AgCl and Ag^0 species were deposited onto TF successfully, and the obtained S-CTF showed improved visible light absorption due to the surface plasmon resonance of Ag^0. In the photocatalytic degradation of X-3B, S-CTF exhibited significantly enhanced activities under separate visible or UV light irradiation, in comparison to TF.

Keywords: Ag/AgCl@TiO_2 fibers; plasmonic photocatalyst; photodegradation

1. Introduction

As a potential technology, photocatalytic oxidation is widely applied in water treatment [1,2] and energy conversion area [3,4]. TiO_2 is considered to be one of the most promising semiconductor photocatalysts due to its low cost, chemical stability and non-toxicity [5]. However, its large band gap (3.2 eV) and high recombination rate of photo-generation carrier [6] limit its applications as an efficient and visible-light driven photocatalyst. Numerous strategies have been explored to enhance its activity, especially doping with nonmetal elements (N and S, etc.) [7,8], coupling with other semiconductors (GO and $BiVO_4$, etc.) [9,10], and depositing with noble metals (Au and Ag, etc.) [11–14]. Ag^0 nanoparticles-modified TiO_2 exhibits excellent activity under visible light resulting from the surface plasmon resonance (SPR) [15,16], which is induced by the nano-size and morphology of Ag^0 [17,18].

Kakuta et al. [19] observed that Ag^0 species were formed on the surface of AgBr under ultraviolet (UV) irradiation. Afterward, Huang et al. [20] found that the modification of TiO_2 with Ag/AgCl obviously improved its photocatalytic activity. However, previous research has mainly focused on the fabrication of nano-sized Ag/AgCl/TiO_2 catalysts, such as nanoparticles [21,22], nanospheres [23], nanoarrays [20,24] and nanofibers [25]. These nano-sized catalysts are difficult to separate directly

from post-slurry for recycling. Therefore, it is crucial to develop an easily recycled catalyst with a macroscopic shape and self-supporting structure. TiO_2 continuous fibers, fabricated be our group using sol-gel and force spinning method, is a promising strategy.

In addition, for most studies on Ag/AgCl-deposited TiO_2, HCl [26] or cetyltrimethylammonium chloride (CTAC) [27] were employed as chlorine sources, which were costly, toxic and harmful to environment. Hence, it is necessary to explore low-cost and non-toxic alternative sources. The cheap and extensive $TiCl_4$ can be employed as a Ti source for TiO_2 fabrication. However, its hydrolytic process is accompanied with the formation of hazardous HCl [28,29]. For this purpose, Xu et al. [30] reported a method in which NaOH was used to neutralize the produced HCl and form NaCl during the hydrolysis of $TiCl_4$. This significant improvement allows us to recycle the produced NaCl, and also invites the investigation of the feasibility of using the NaCl as Cl source for Ag/AgCl deposition.

In this study, TiO_2 fibers (TF) with a macroscopic shape were fabricated by a sol-gel method according to the previously developed TiO_2 continuous fibers [31], and Ag/AgCl nanoparticles were deposited on TF by an impregnation-precipitation-photoreduction method [20]. $TiCl_4$ served as the Ti source for TF, and NaOH aqueous solution was utilized to hydrolyze $TiCl_4$, neutralize the produced HCl and form NaCl. The recycled NaCl was employed as a chlorine source for Ag/AgCl deposition. The morphology, textural properties, chemical component and optical property of Ag/AgCl@TiO_2 fibers (S-CTF) were analyzed by scanning electron microscopy (SEM), N_2 absorption and desorption isotherms, X-ray diffractometer (XRD), X-ray photoelectron spectroscopy (XPS) and UV-vis spectrophotometer (UV-vis DRS). The photocatalytic activity and stability were evaluated by brilliant red X-3B degradation under visible and UV light.

2. Results and Discussion

2.1. Morphology and Textural Properties

2.1.1. SEM

Figure 1 presents typical SEM images of TF, AgCl@TiO_2 fibers (CTF) and S-CTF. The diameters of the fibers are about 30 μm. In Figure 1a,c,e, the surface of TF is homogeneous and smooth, while the surface of CTF and S-CTF are rough. Local enlarged images of TF, CTF and S-CTF are shown in Figure 1b,d,f, in which the porous structure that formed by the agglomeration of TiO_2 nanoparticles can be observed. AgCl particles with diameters less than 300 nm (Figure 1d) were successfully deposited on TF. However, there is no significant difference between the SEM images of CTF and S-CTF. The existence of Ag^0 cannot be observed through SEM, but will be confirmed by XRD, XPS and UV-vis DRS.

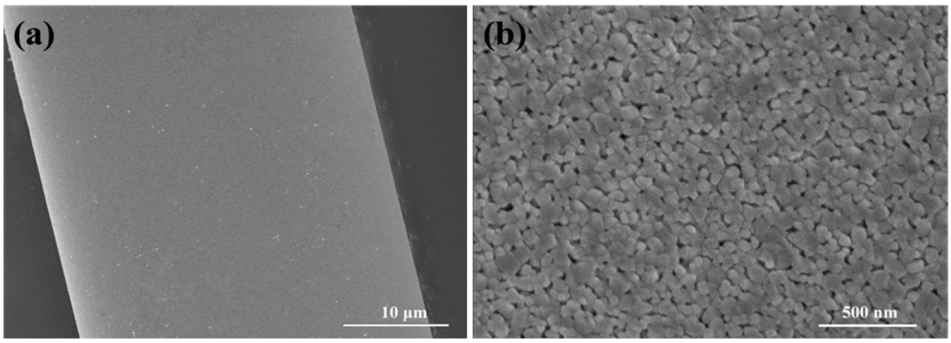

Figure 1. *Cont.*

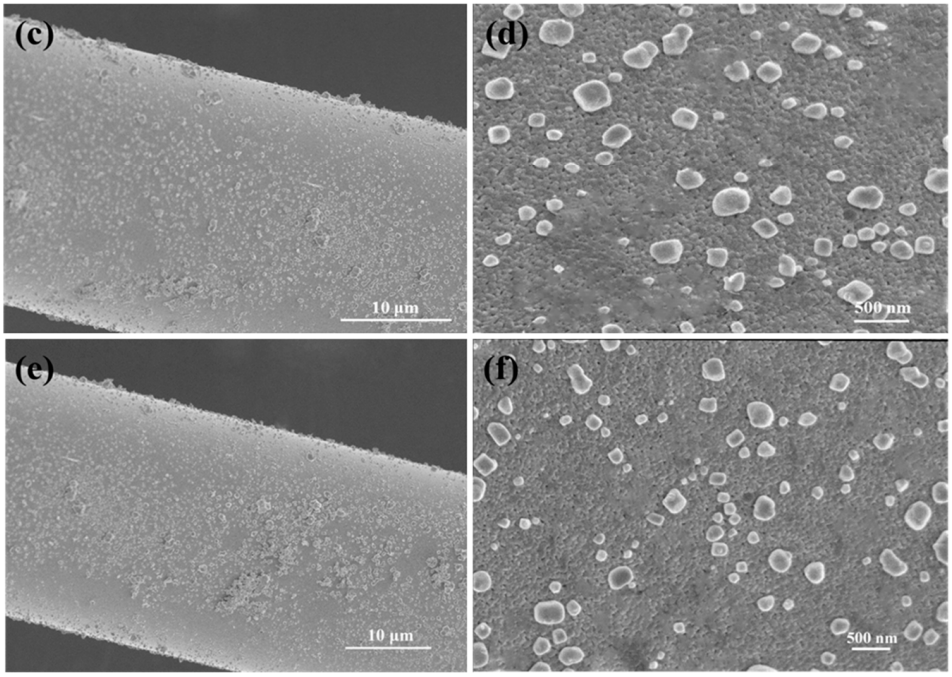

Figure 1. SEM images of TF (**a**,**b**), CTF (**c**,**d**) and S-CTF (**e**,**f**).

2.1.2. Textural Properties

The textural parameters of TF and S-CTF are presented in Table 1. After heat treatment, the Brunauer-Emmett-Teller (BET) surface area of TF increases from 16.0 of precursor fibers (PF) to 27.9 m^2 g^{-1} (TF), due to the removal of organic matters and the formation of porous structure. With Ag/AgCl particles deposited on TF, the surface area of S-CTF increases to 30.6 m^2 g^{-1}, which is due to its rough surface [32], as shown in Figure 1.

Table 1. Textural Parameters of TF (TiO_2 fibers) and S-CTF (Ag/AgCl@TiO_2 fibers).

Samples	BET Surface Area (m^2 g^{-1})	Pore Volume (cm^3 g^{-1})	Pore Diameter (nm)
TF	27.9	0.111	16.7
S-CTF	30.6	0.074	10.8

N_2 absorption and desorption isotherms of TF and S-CTF are shown in Figure 2a. Isotherms of TF and S-CTF belong to *typical IV* adsorption behavior and *Type H1* hysteresis loop, according to International Union of Pure and Applied Chemistry (IUPAC) classification [33], which is consistent with pores with homogeneous and spindle cylindrical shapes. This reveals the formation of a mesoporous structure by the heat treatment. According to the pore-size distribution isotherms (Figure 2b), S-CTF shows narrower pore-size distribution (3–22 nm) and smaller average pore size (10.8 nm) than TF (5–40 nm and 16.7 nm). Hence, S-CTF (0.111 cm^3 g^{-1}) possesses smaller pore volume compared to TF (0.074 cm^3 g^{-1}). The decrease of average pore size and volume results from the deposition of nano-sized Ag/AgCl particles into macro-sized pores. In addition, S-CTF shows bimodal porous structure with two pore-size distribution peaks at 3.80 and 10.8 nm, which has also resulted from the pore size narrowing by AgCl deposition. The enlarged surface area and narrowed bimodal pore-size distribution obtained by S-CTF are both benefited to dye adsorption [34,35].

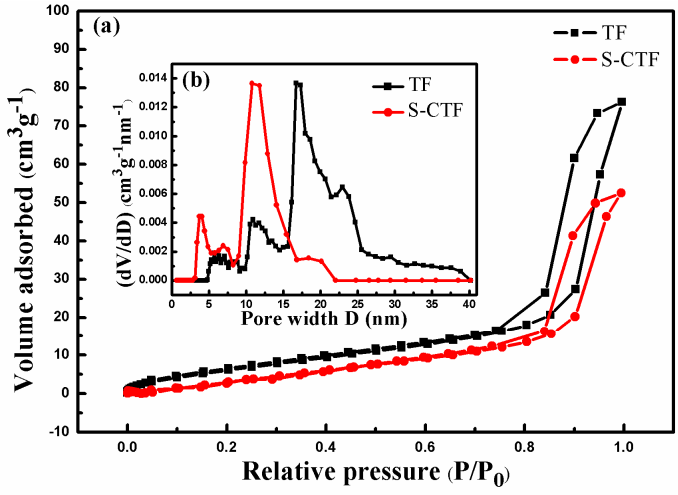

Figure 2. N_2 adsorption-desorption isotherms (**a**) and pore-size distribution (**b**) of TF and S-CTF.

2.2. XRD

Figure 3a shows XRD patterns of NaCl produced in the neutral reaction of NaOH and HCl. According to Joint Committee on Powder Diffraction Standards (JCPDS) standards, its crystal form is confirmed to be halite NaCl by diffraction peaks at 27.4°, 31.7°, 45.4°, 53.7°, 56.4°, 66.2° and 57.3°. XRD patterns of AgCl, Ag/AgCl, TF, CTF and S-CTF are shown in Figure 3b. Diffraction peaks of TF, Ag@TiO_2(CTF) and S-CTF at about 25.3°, 37.8°, 48.1°, 53.9°, 55.1°, 62.7°, 68.7°, 70.3° and 75.1° belong to (101), (004), (200), (105), (211), (204), (116), (220) and (215) reflections [36] of anatase TiO_2 (JCPDS No. 21-1272), while diffraction peaks of AgCl, Ag/AgCl, CTF and S-CTF at about 27.9°, 32.3°, 46.3°, 54.9°, 57.5°, 67.5° and 76.7° are in accordance with the (111), (200), (220), (311), (222), (400) and (420) planes [37] of cubic phase AgCl (JCPDS No. 31-1238). A weak diffraction peak at $2\theta = 38.3°$ of cubic phase Ag (JCPDS No. 65-2871) in Ag/AgCl confirmed the successful photoreduction of AgCl and the formation of Ag^0. However, no obvious diffraction peak of Ag^0 occurred in S-CTF, which is due to the peak overlap with anatase (at about $2\theta = 37.8°$) and its high dispersion. Otherwise, anatase peaks of CTF and S-CTF show about 0.45 and 0.2 shifts compared with TF (inset in Figure 3b), which is mainly caused by the combination of AgCl and the formation of Ag^0. The shift of anatase peaks towards higher angles indicate a lattice expansion [38] due to the AgCl and Ag^0 nanoparticles in the interlayer space of anatase gains agglomerated fibers.

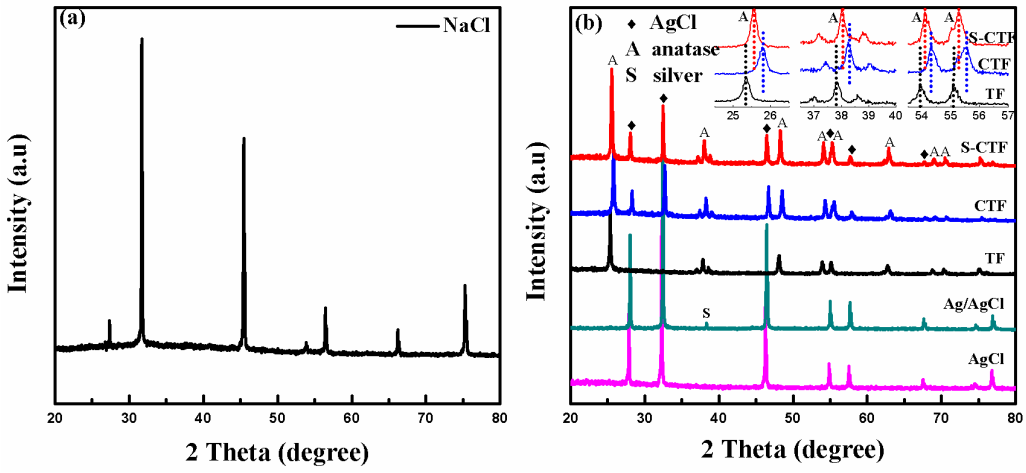

Figure 3. XRD patterns of NaCl separated from reaction solution (**a**), AgCl, Ag/AgCl, TF, CTF and S-CTF (**b**).

2.3. XPS

The XPS survey spectrum of S-CTF (Figure 4a) shows all peaks of Ti, O, Ag, Cl and C elements. The peak for C 1s at 284.6 eV is mainly from the adventitious hydrocarbon, due to the XPS instrument itself. The result of the survey of the XPS spectrum is consistent with the XRD results.

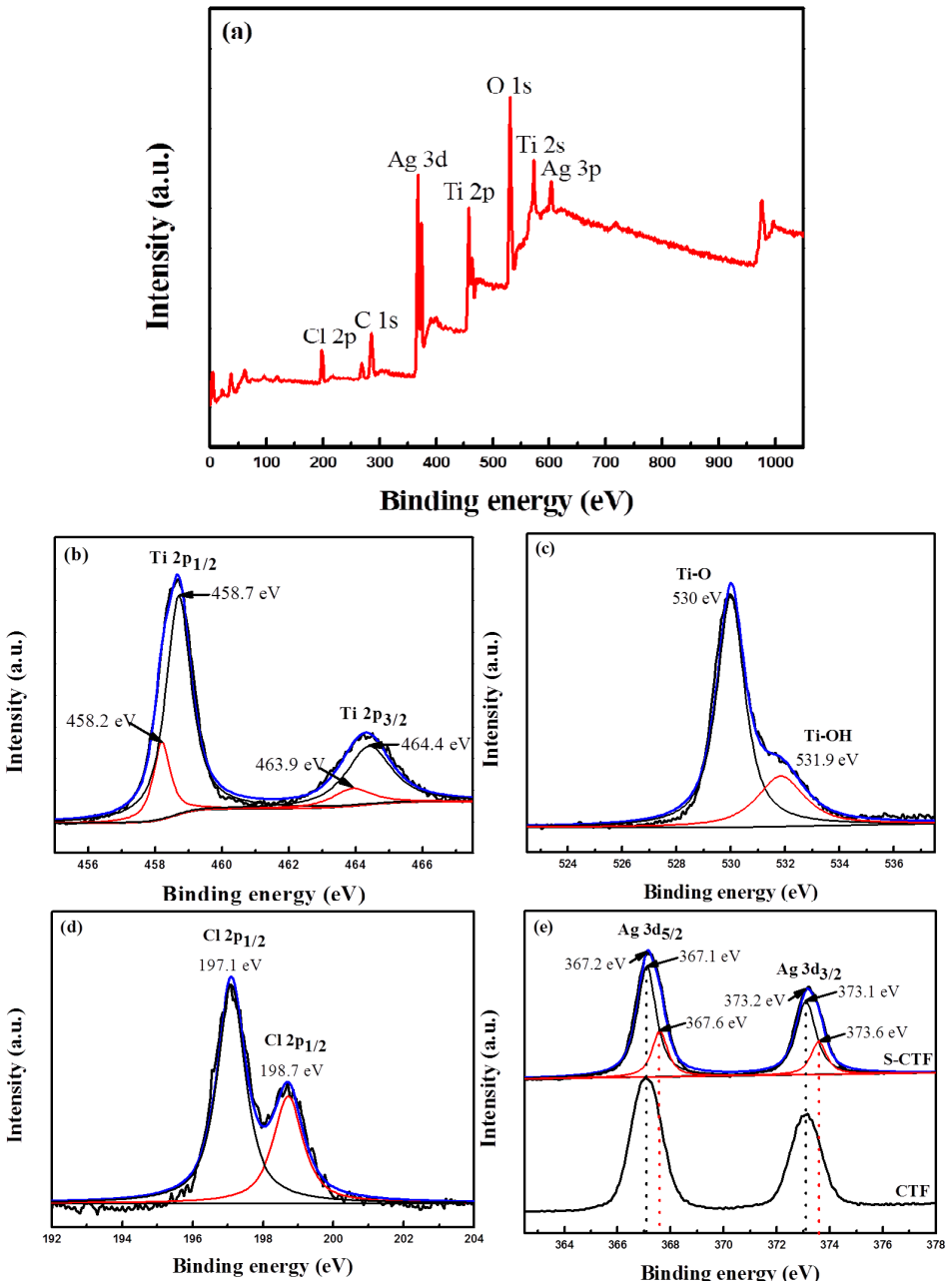

Figure 4. XPS spectra of all elements of S-CTF (**a**) and the band energy of Ti 2p (**b**), O 1s (**c**), Cl 2p (**d**) and Ag 3d (**e**).

The valence state of Ti, O, Cl and Ag in S-CTF are investigated by the high-resolution XPS spectrum (Figure 4b–e). As shown in Figure 4b, the binding energy at 458.6 and 464.6 eV of Ti $2p_{1/2}$ and Ti $2p_{3/2}$ are lower than those of pure TiO_2 (459.4 and 464.7 eV) [39]. The curve resolution of the Ti 2p signal of S-CTF indicates four different peaks. The peaks at binding energies of 458.2 and 463.9 eV belong to Ti $2p_{1/2}$ and Ti $2p_{3/2}$ of Ti^{3+}, while the other two peaks at 458.7 and 464.4 eV belong to Ti $2p_{1/2}$ and Ti $2p_{3/2}$ of Ti^{4+} [40]. Ti^{3+} (and oxygen vacancy) in S-CTF was produced during the heat

treatment by the reduction of TF (the removal of partial lattice oxygen) with organic matters in steam as a reducing atmosphere. The O 1s region is decomposed into two peaks at 530 and 531.9 eV (Figure 4b). The two kinds of oxygen contributions are ascribed to Ti–O in TiO_2 and the OH in Ti–OH (adsorbed water on the surface of S-CTF) [35]. In Figure 4c, two signal peaks of Cl $2p_{1/2}$ and Cl $2p_{3/2}$ at binding energy of 197.1 and 198.7 eV with a separation of 1.6 eV confirmed the Cl^- from AgCl [41]. The Ag 3d region is decomposed into four peaks (Figure 4e). Binding energy peaks at 367.6 and 373.6 eV are ascribed to Ag^0, while 367.1 and 373.1 eV correspond to Ag^+ in AgCl particles [26,42]. The difference of binding energy (0.1 eV) between CTF and S-CTF also indicates the formation of Ag^0. According to the results of XPS, the detail atomic percentages of Ag, AgCl, and TiO_2 on the surface of S-CTF were about 8.5%, 40.7% and 51.8%, respectively. Moreover, the interaction among Ag, AgCl and TiO_2 [43] is further confirmed by the binding energy shifts peaks for all elements compared with standard values.

The crystal structure and chemical component of S-CTF are investigated by XRD and XPS analysis. The formation of Ag^0 and Ti^{3+} would enhance the optical property of S-CTF.

2.4. UV-Vis DRS

Compared with TF, S-CTF exhibits a slight enhancement in the UV light region (<400 nm) and considerable enhancement in the visible light region (>400 nm) (Figure 5). CTF shows the highest absorption in the UV light region among the samples, even higher than S-CTF. With the photoreduction of AgCl and the formation of Ag^0, the absorption of UV light decreases but is still higher than TF. Therefore, the enhancement of absorption in the UV light region can be ascribed to the combination of TF and AgCl with excellent UV light absorption. Because of the formation of Ti^{3+} and oxygen vacancy, TF possesses localized states below the conduct bind(CB) minimum and shows expected light absorption in the visible light region [39,44,45]. TF shows an absorption band edge at about 400 nm, and the absorption band edge of CTF and S-CTF (at about 420 nm) shows an expected red-shift, in comparison to TF. Compared with Ag/AgCl, S-CTF almost retains the same absorption intensity in the visible light region, illustrating that the composition of TF and Ag/AgCl has no influence on the light absorption of Ag/AgCl. Obviously, an additional absorption for S-CTF which was observed in the region of 400–600 nm, which is attributed to the SPR of Ag^0 nanoparticles [41]. The broad and enhanced absorption in the visible light region is also confirmed the formation of Ag^0 [46,47]. These evidences of Ag^0 formation are consistent with the results of XPS.

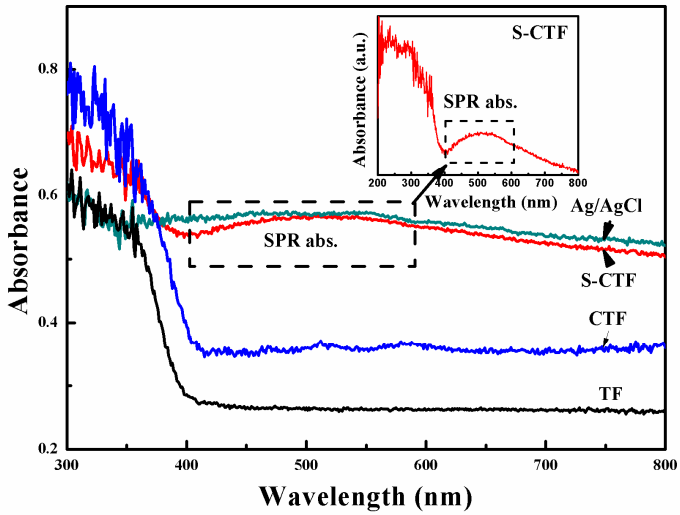

Figure 5. UV-vis diffuse reflectance spectrum of Ag/AgCl, TF, CTF and S-CTF.

2.5. Photocatalytic Activity

To evaluate the effect of the interaction between Ag/AgCl and the TF surface, Ag/AgCl/precursor fibers (S-CPF) were prepared. To investigate the influence of photosensitization and to confirm the photoactivity of TF, pure TiO_2 fibers (pure-TF) were also prepared by PF through heat treatment (the heating program was the same as that used for TF preparation) in O_2 atmosphere with the flow rate at 0.5 L/min. The photocatalytic activities of pure-TF, TF, CTF, S-CPF and S-CTF toward X-3B degradation under visible and UV light are shown in Figure 6.

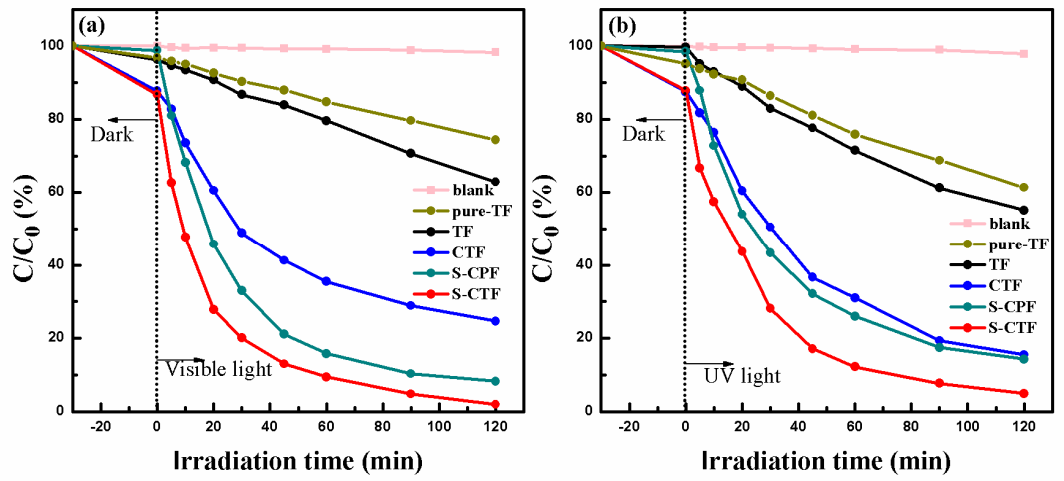

Figure 6. Photocatalytic degradation of 100 mL X-3B (20 mg L^{-1}) over pure-TF TF, CTF, S-CPF and S-CTF (0.05 g) under visible light (**a**) and ultrasonic light (**b**) with blank control groups.

After dark treatment for 30 min (Figure 6), S-CTF and CTF (about 12%) have higher X-3B adsorption than pure-TF and TF (about 4%). Nearly no adsorption is observed for S-CPF. The enhancement for X-3B adsorption is a result of the enlarged surface area and narrowed bimodal mesoporous structure after AgCl deposition.

The degradation efficiencies within 120 min under visible light (Figure 6a) follow an order of pure − TF (25.6%) < TF (37.1%) < CTF (73.4%) < S − CPF (91.8%) < S − CTF (98.1%). After 120 min, the degradation efficiency by pure-TF was 25.6%, which was lower than TF (37.1%). The degradation of X-3B by pure-TF can be attributed to the photosensitization of dye, and the degradation elevation of TF can be attributed to the existence of Ti^{3+} and the optical absorption of visible light. CTF shows high photoactivity due to the reduction of AgCl and the formation Ag^0 as the photoreaction progressed [32]. Because of the strong SPR of Ag^0, S-CPF and S-CTF exhibit much higher degradation efficiencies than TF and CTF. The highest efficiency by S-CTF is ascribed to the better separation capacity of photo-generated carriers than S-CPF.

Under UV light, the degradation efficiencies of X-3B (Figure 6b) for 120 min are displayed as following sequence: pure − TF (38.6%) < TF (44.8%) < CTF (84.5%) < S − CPF (85.7%) < S − CTF (95.1%). The higher efficiency of TF than pure-TF can be attributed to the more efficient carrier separation with oxygen vacancy in TF. CTF and S-CPF exhibit much higher activity than TF. Compared with X-3B degradation efficiency under visible light, the efficiency elevation by CTF results from the excitement of AgCl and the higher activity of TF. Since Ag^0 possesses the capacity to trap electrons [48], S-CTF shows the highest degradation efficiency.

The stability of S-CTF is further measured by a recycling experiment. After five runs, the degradation efficiencies of S-CTF under visible and UV light are still as high as 90.8% and 87.5%. The catalyst is stable enough, even considering the inevitable loss of weight during each cycle.

2.6. Photocatalytic Mechanism

2.6.1. Photoluminescence (PL)

The recombination of the photoinduced electrons and holes is a crucial factor in a photocatalytic reaction for the decrease of quantum yield. The efficiencies of photo-generated carriers [12,49,50] are explained by PL analysis. A strong emission peak of TF is observed at about 400 nm with the excitation wavelength at 325 nm (Figure 7), which indicates the direct recombination of electrons and holes. No obvious emission peak is observed in PL spectra of Ag/AgCl and S-CTF, while S-CTF shows lower PL intensity than Ag/AgCl, indicating its better separation capacity caused by the interaction among Ag, AgCl and TiO_2. The results of PL analysis are in accordance with the results of XRD and XPS. Otherwise, an additional peak of TF (at about 470 nm), belonging to oxygen vacancy [51], further confirms the formation of oxygen vacancy and Ti^{3+}.

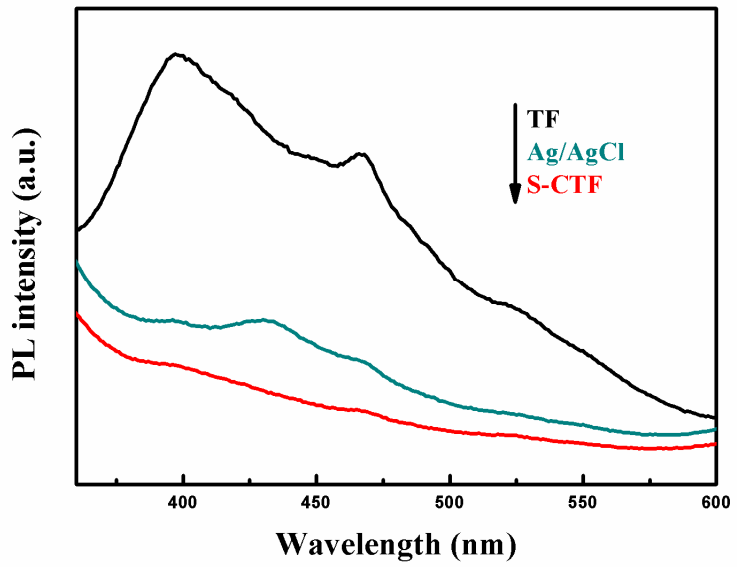

Figure 7. Photoluminescence spectra of TF, Ag/AgCl and S-CTF.

2.6.2. Photocatalytic Mechanism

To better understand the photocatalytic mechanisms of S-CTF and to investigate the main oxidative species during the photodegradation of X-3B, tert-butyl alcohol (TBA), $AgNO_3$, disodium ethylenediaminetetraacetate (EDTA-Na_2) and benzoquinone (BQ) are used as •OH, electrons, holes and $\bullet O_2^-$ quenchers. Under visible light irradiation, the degradation efficiency of X-3B decreases from 98.0% to 87.2% (TBA), 74.6% ($AgNO_3$), 43.9% (EDTA-Na_2) and 36.7% (BQ). Under UV light irradiation, the degradation efficiency of X-3B reduces from 95.1% to 85.5% (TBA), 82.2% ($AgNO_3$), 65.5% (EDTA-Na_2) and 40.3% (BQ). These results illustrate that the critical species under visible light are holes and $\bullet O_2^-$, while the most critical specie under UV light is $\bullet O_2^-$.

The photocatalytic mechanism of S-CTF under visible light is shown in Figure 8a. Ag^0 exhibits strong SPR and generates electron-hole pairs under visible irradiation [52]. TF with the existence of Ti^{3+} is also excited under visible light. With the efficient interaction of Ag^0, AgCl and TF, the plasmon-excited electrons are injected into the conduction band (CB) of TF [20,45] easily, and subsequently produce $\bullet O_2^-$ with O_2. Meanwhile, the photo-excited holes are transferred to the surface of AgCl, X-3B molecules [20,32] and the value band (VB) of TF. The efficient separation of carriers among Ag, AgCl and TF is confirmed by PL spectra. Holes participate in the degradation of organic dyestuff by formation of Cl^0 and •OH. Firstly, the holes transfer to AgCl and convert Cl^- ions into Cl^0 atoms [53]. The Cl^0 species oxidize the X-3B molecules and form AgCl. These reactions ensure that Ag/AgCl and S-CTF remain stable during the photodegradation process [16,20,37]. Secondly, the

holes generate by TF yield •OH radicals or degrade organic pollutants directly. The photosensitization of X-3B [54] (generated electrons can inject into the CB of TF from excited dyes) also can be regarded as an advantage in its degradation.

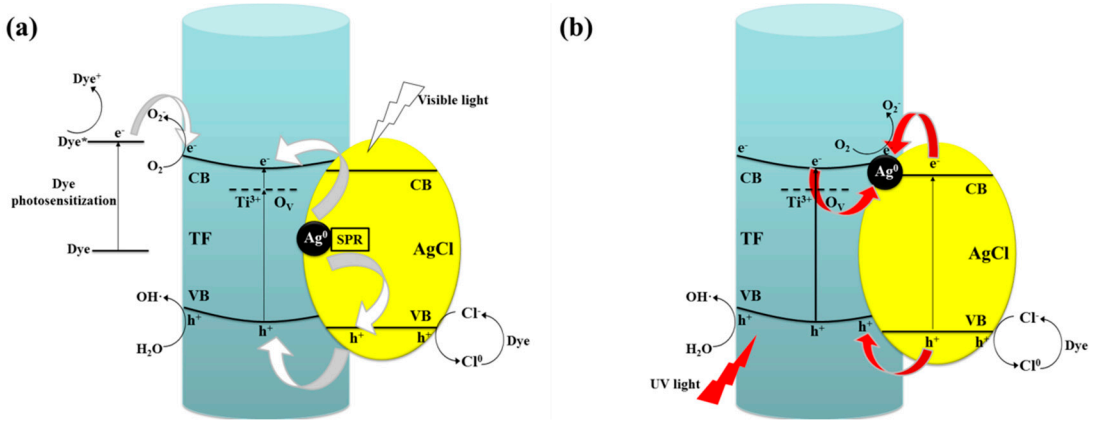

Figure 8. Photocatalytic mechanisms of S-CTF under visible (**a**) and UV (**b**) light irradiation.

Figure 8b shows the photocatalytic mechanism of S-CTF under UV light. The transformation of electron-hole pairs is different from visible irradiation. According to the CB and VB edge potentials of TiO_2 (−0.29 and 2.91 eV [40]) and AgCl (0.09 and 3.16 [55]), both TiO_2 and AgCl are excited under UV irradiation. The generated holes of AgCl can easily inject into the VB of TF [41], and then yield •OH with adsorbed water molecules, or directly degrade organic pollutants such as the holes generated by TF. The holes also yield Cl^0 and reduce this to Cl^- via the same route under visible irradiation. The electrons generated from the CB of TF and AgCl transfer to Ag^0, which serves as an electron trap under UV irradiation [48,56]. These electrons participate in the formation of $\bullet O_2^-$ radicals. Moreover, the oxygen vacancy in TF is also beneficial to trap electrons and promote their separation under visible or UV light irradiation [40].

3. Materials and Methods

3.1. Chemicals

$TiCl_4$, acetylacetone (AcAc), triethylamine (TEA), methyl alcohol (MeOH), tetrahydrofuran (THF), NaOH and $AgNO_3$ were purchased from Sinopharm International Co. Ltd. (Shanghai, China). Brilliant red X-3B was purchased from Shanghai Dyestuff Chemical Plant. All of the experiments in this research used deionized water. All of the chemical reagents were analytical grade, and were used without further purification.

3.2. Preparation of Catalysts

TiO_2 fibers (TF) were synthesized by a sol-gel method combined with centrifugal spinning technique, followed by stage-temperature-programmed heat treatment in a steam atmosphere. The hydrolysis of $TiCl_4$ (10 mL in MeOH) was carried out by mixing 4 mL NaOH aqueous solution (0.5 g mL^{-1}) and 25 mL MeOH under ice-cold conditions. The reaction can be expressed as: $TiCl_4 + H_2O \rightarrow TiO_2 + HCl$. During the reaction, NaOH neutralized the produced HCl to form NaCl, and the formed NaCl was supersaturated and precipitated due to its relatively small saturation in MeOH. Then, NaCl was filtered and collected for Ag/AgCl deposition. The TiO_2 was chelated by AcAc to form a spinning solution. After the centrifugal spinning, precursor fibers (PF) were obtained and converted to TF by the heat treatment in steam as a reducing atmosphere. The detailed heat treatment program is shown in Table 2.

Table 2. Program of Segmented Heating.

Temperature (°C)	Heating Rate (°C min^{-1})	Time (min)
25–95	1.67	42
95–250	1.29	120
250–350	0.83	120
350–550	5.00	40
550–600	0.83	60
600–600	-	120

Ag/AgCl@TiO_2 fibers (S-CTF) were prepared by the deposition of Ag/AgCl on TF. The recycled NaCl and $AgNO_3$ were prepared into impregnation liquids. TF was soaked in 1 M NaCl and 0.1 M $AgNO_3$ solution for 10 min prior for AgCl deposition, and washed by deionized water to rinse the excess elements after each soak. This process was repeated for five trials. After being dried at 353 K, the prepared AgCl@TiO_2 fibers (CTF) were irradiated under a 1000 W xenon lamp (50 cm away from the light source) for 10 min to reduce partial Ag^+ to Ag^0 on the surface of the AgCl particles.

3.3. Characterization of Catalysts

To observe the structure and morphology of the prepared samples, scanning electron microscopy (SEM, JSM 6700F, JEOL, Tokyo, Japan) was employed. A Quadrasorb SI-MP system (Quantachrome, Boynton Beach, FL, USA) was used to acquire the N_2 adsorption-desorption isotherms. The Brunauer-Emmett-Teller (BET) specific surface area was detected by a multipoint BET method, and the adsorption data was acquired in the relative pressure (P/P_0) range of 0.05–0.3. The pore size distribution was calculated by employing the Density Functional Theory (DFT). The average pore size and pore volume data were obtained by the N_2 adsorption volume with the relative pressure at 0.991. An X-ray diffractometer (XRD, D8 Advance, Bruker AXS GmbH, Karlsruhe, Germany) was employed to determine the crystal structure of the prepared photocatalysts. An ESCALAB 250 spectrometer (Thermo Electron Corp., Cramlington, UK) with an Al KR source and a charge neutralizer was used to perform the X-ray photoelectron spectroscopy (XPS). All the spectra were calibrated to the C 1s peak at 284.6 eV. A UV-vis spectrophotometer (UV-3100, Shimadzu, Kyoto, Japan) was employed to investigate the light absorption property of the photocatalysts samples. To measure the solid-state UV-vis diffuse reflectance spectra, an integrating sphere attachment was equipped with $BaSO_4$ as a background in room temperature and air conditions. A fluorescence spectrometer (F-4600, Hitachi, Tokyo, Japan) was used to measure the photoluminescence (PL) spectra of all the samples.

3.4. Photoactivity Studies

The photocatalytic performance of S-CTF was evaluated by the decolorization of X-3B under visible and UV light. A 1000 W Xe lamp inserted by a glass optical filter to cut off short wavelength components (λ < 420 nm) and a 250 W high pressure mercury lamp with a maximum wavelength at 365 nm served as visible and UV light sources, respectively. Before the photocatalytic reaction, 50 mg of each sample was added to 200 mL X-3B aqueous solution (20 mg/L) in an open fixed-bed photo-reactor [57] which was cooled through the circulation of water at 293 K. To establish the adsorption/desorption equilibrium, the photo-reactor was stirred in dark conditions for 30 min. Then, the reactor was placed under visible and UV irradiation with the irradiation intensity at the surface of the dye solution being 250 W m^{-2} and 15 W m^{-2}, respectively, and cycled by a peristaltic pump with a flow rate of 20 mL min^{-1}. During the photocatalytic reaction, 3 mL reaction solution was taken at each interval and filtrated through a 0.45 μm syringe filter. A UV-vis 1601 spectrophotometer (Shimadzu, Japan) was used to measure the concentration of X-3B by the variation of the maximum absorption wavelength (536 nm) of filtrate which was determined. The degradation efficiency was calculated by the formula $R = (1 - C/C_0) \times 100\%$, in which C and C_0 stood for the initial concentration and the concentration of dye at each moment in the reaction, respectively.

Species capture experiments were performed to investigate the mechanism of TF. 10.0 mM of TBA), BQ, $AgNO_3$ and EDTA-Na_2 were added into X-3B solution acting as •OH, $\bullet O_2^-$, electrons and holes scavengers. The reaction processes are same as that of the degradation reaction by S-CTF.

4. Conclusions

In summary, the plasmonic photocatalyst S-CTF was prepared by the gel-sol method to synthesize TF, and the impregnation-precipitation-photoreduction method to deposit Ag/AgCl particles on the produced TF. AgCl particles were deposited on TF with recycled NaCl as Cl sources, which were produced in the hydrolysis of $TiCl_4$ by NaOH aqueous solution. The improved dye adsorption compared to TF was due to the enlarged specific surface area and narrowed pore-size distribution after AgCl deposition. The increased photocatalytic efficiency resulted from the SPR of Ag^0, enhanced light absorption, narrowed band gap and efficient charge separation. With its outstanding photocatalytic performance and high stability, S-CTF is a promising application in organic pollutant treatment and wastewater purification. Furthermore, this mild, less-toxic and lower-cost synthesis process is accordance with environmental protection concepts.

Acknowledgments: This work was supported by the Natural Science Foundation of Shandong Province, China (No. ZR2011BM005) and the Fundamental Research Funds of Shandong University (No. 2015JC022).

Author Contributions: Xinhan Miao and Xiuyan Jie prepared the catalysts; Xinhan Miao and Xinde Hu performed the experiment; Xinhan Miao and Xiyue Zheng prepared the manuscript; Qingzhe Zhang directed the manuscript drafting; Nan Bao directed the project.

Conflicts of Interest: The authors declare no conflict of interest.

References

1. Legrini, O.; Oliveros, E.; Braun, A.M. Photochemical processes for water treatment. *Chem. Rev.* **1993**, *93*, 671–698. [CrossRef]
2. Chong, M.N.; Jin, B.; Chow, C.W.K.; Saint, C. Recent developments in photocatalytic water treatment technology: A review. *Water Res.* **2010**, *44*, 2997–3027. [CrossRef] [PubMed]
3. Liu, G.; Yin, L.-C.; Wang, J.; Niu, P.; Zhen, C.; Xie, Y.; Cheng, H.-M. A red anatase TiO_2 photocatalyst for solar energy conversion. *Energy Environ. Sci.* **2012**, *5*, 9603–9610. [CrossRef]
4. Kudo, A. Development of photocatalyst materials for water splitting with the aim at photon energy conversion. *J. Ceram. Soc. Jpn.* **2001**, *109*, S81–S88. [CrossRef]
5. Pelaez, M.; Nolan, N.T.; Pillai, S.C.; Seery, M.K.; Falaras, P.; Kontos, A.G.; Dunlop, P.S.M.; Hamilton, J.W.J.; Byrne, J.A.; O'Shea, K.; et al. A review on the visible light active titanium dioxide photocatalysts for environmental applications. *Appl. Catal. B Environ.* **2012**, *125*, 331–349. [CrossRef]
6. Choi, W.; Termin, A.; Hoffmann, M.R. The role of metal ion dopants in quantum-sized TiO_2: Correlation between photoreactivity and charge carrier recombination dynamics. *J. Phys. Chem.* **1994**, *98*, 13669–13679. [CrossRef]
7. Asahi, R.; Morikawa, T.; Ohwaki, T.; Aoki, K.; Taga, Y. Visible-light photocatalysis in nitrogen-doped titanium oxides. *Science* **2001**, *293*, 269–271. [CrossRef] [PubMed]
8. Liu, Y.; Liu, J.; Lin, Y.; Zhang, Y.; Wei, Y. Simple fabrication and photocatalytic activity of S-doped TiO_2 under low power led visible light irradiation. *Ceram. Int.* **2009**, *35*, 3061–3065. [CrossRef]
9. Chen, C.; Cai, W.; Long, M.; Zhou, B.; Wu, Y.; Wu, D.; Feng, Y. Synthesis of visible-light responsive graphene oxide/TiO_2 composites with p/n heterojunction. *ACS Nano* **2010**, *4*, 6425–6432. [CrossRef] [PubMed]
10. Bao, N.; Yin, Z.; Zhang, Q.; He, S.; Hu, X.; Miao, X. Synthesis of flower-like monoclinic $BiVO_4$/surface rough TiO_2 ceramic fiber with heterostructures and its photocatalytic property. *Ceram. Int.* **2016**, *42*, 1791–1800. [CrossRef]
11. Yang, Y.; Wen, J.; Wei, J.; Xiong, R.; Shi, J.; Pan, C. Polypyrrole-decorated Ag-TiO_2 nanofibers exhibiting enhanced photocatalytic activity under visible-light illumination. *ACS Appl. Mater. Interfaces* **2013**, *5*, 6201–6207. [CrossRef] [PubMed]
12. Li, F.B.; Li, X.Z. Photocatalytic properties of gold/gold ion-modified titanium dioxide for wastewater treatment. *Appl. Catal. A Gen.* **2002**, *228*, 15–27. [CrossRef]

13. Zhang, Q.; Thrithamarassery Gangadharan, D.; Liu, Y.; Xu, Z.; Chaker, M.; Ma, D. Recent advancements in plasmon-enhanced visible light-driven water splitting. *J. Materiomics* **2017**, *3*, 33–50. [CrossRef]
14. Kumar, R.; El-Shishtawy, M.R.; Barakat, A.M. Synthesis and characterization of Ag-Ag_2O/TiO_2@polypyrrole heterojunction for enhanced photocatalytic degradation of methylene blue. *Catalysts* **2016**, *6*, 76. [CrossRef]
15. Awazu, K.; Fujimaki, M.; Rockstuhl, C.; Tominaga, J.; Murakami, H.; Ohki, Y.; Yoshida, N.; Watanabe, T. A plasmonic photocatalyst consisting of silver nanoparticles embedded in titanium dioxide. *J. Am. Chem. Soc.* **2008**, *130*, 1676–1680. [CrossRef] [PubMed]
16. Wang, P.; Huang, B.; Qin, X.; Zhang, X.; Dai, Y.; Wei, J.; Whangbo, M.-H. Ag@AgCl: A highly efficient and stable photocatalyst active under visible light. *Angew. Chem. Int. Ed.* **2008**, *47*, 7931–7933. [CrossRef] [PubMed]
17. Jin, R.; Cao, Y.; Mirkin, C.A.; Kelly, K.L.; Schatz, G.C.; Zheng, J.G. Photoinduced conversion of silver nanospheres to nanoprisms. *Science* **2001**, *294*, 1901–1903. [CrossRef] [PubMed]
18. Jain, P.K.; Lee, K.S.; El-Sayed, I.H.; El-Sayed, M.A. Calculated absorption and scattering properties of gold nanoparticles of different size, shape, and composition: Applications in biological imaging and biomedicine. *J. Phys. Chem. B* **2006**, *110*, 7238–7248. [CrossRef] [PubMed]
19. Kakuta, N.; Goto, N.; Ohkita, H.; Mizushima, T. Silver bromide as a photocatalyst for hydrogen generation from CH_3OH/H_2O solution. *J. Phys. Chem. B* **1999**, *103*, 5917–5919. [CrossRef]
20. Yu, J.; Dai, G.; Huang, B. Fabrication and characterization of visible-light-driven plasmonic photocatalyst Ag/AgCl/TiO_2 nanotube arrays. *J. Phys. Chem. C* **2009**, *113*, 16394–16401. [CrossRef]
21. Guo, J.-F.; Ma, B.; Yin, A.; Fan, K.; Dai, W.-L. Highly stable and efficient Ag/AgCl@TiO_2 photocatalyst: Preparation, characterization, and application in the treatment of aqueous hazardous pollutants. *J. Hazard. Mater.* **2012**, *211–212*, 77–82. [CrossRef] [PubMed]
22. Hu, C.; Lan, Y.; Qu, J.; Hu, X.; Wang, A. Ag/AgBr/TiO_2 visible light photocatalyst for destruction of azodyes and bacteria. *J. Phys. Chem. B* **2006**, *110*, 4066–4072. [CrossRef] [PubMed]
23. Nunes, D.; Pimentel, A.; Santos, L.; Barquinha, P.; Fortunato, E.; Martins, R. Photocatalytic TiO_2 nanorod spheres and arrays compatible with flexible applications. *Catalysts* **2017**, *7*, 60. [CrossRef]
24. Liao, W.; Zhang, Y.; Zhang, M.; Murugananthan, M.; Yoshihara, S. Photoelectrocatalytic degradation of microcystin-LR using Ag/AgCl/TiO_2 nanotube arrays electrode under visible light irradiation. *Chem. Eng. J.* **2013**, *231*, 455–463. [CrossRef]
25. Wang, D.; Li, Y.; Li Puma, G.; Wang, C.; Wang, P.; Zhang, W.; Wang, Q. Ag/AgCl@helical chiral TiO_2 nanofibers as a visible-light driven plasmon photocatalyst. *Chem. Commun.* **2013**, *49*, 10367–10369. [CrossRef] [PubMed]
26. Wang, P.; Huang, B.; Lou, Z.; Zhang, X.; Qin, X.; Dai, Y.; Zheng, Z.; Wang, X. Synthesis of highly efficient Ag@AgCl plasmonic photocatalysts with various structures. *Chem. Eur. J.* **2010**, *16*, 538–544. [CrossRef] [PubMed]
27. Ma, B.; Guo, J.; Dai, W.-L.; Fan, K. Ag-AgCl/WO_3 hollow sphere with flower-like structure and superior visible photocatalytic activity. *Appl. Catal. B Environ.* **2012**, *123–124*, 193–199. [CrossRef]
28. Di Paola, A.; Bellardita, M.; Ceccato, R.; Palmisano, L.; Parrino, F. Highly active photocatalytic TiO_2 powders obtained by thermohydrolysis of $TiCl_4$ in water. *J. Phys. Chem. C* **2009**, *113*, 15166–15174. [CrossRef]
29. Zhu, Y.; Zhang, L.; Gao, C.; Cao, L. The synthesis of nanosized TiO_2 powder using a sol-gel method with $TiCl_4$ as a precursor. *J. Mater. Sci.* **2000**, *35*, 4049–4054. [CrossRef]
30. Xu, H.; Gao, L.; Guo, J. Hydrothermal synthesis of tetragonal barium titanate from barium chloride and titanium tetrachloride under moderate conditions. *J. Am. Ceram. Soc.* **2002**, *85*, 727–729. [CrossRef]
31. Bao, N.; Yin, G.-B.; Wei, Z.-T.; Li, Y.; Ma, Z.-H. Preparation of TiO_2 continuous fibers with oxygen vacancies and photocatalytic activity. *Integr. Ferroelectr.* **2011**, *127*, 97–105. [CrossRef]
32. Zhou, J.; Cheng, Y.; Yu, J. Preparation and characterization of visible-light-driven plasmonic photocatalyst Ag/AgCl/TiO_2 nanocomposite thin films. *J. Photochem. Photobiol. A Chem.* **2011**, *223*, 82–87. [CrossRef]
33. Dai, Y.; Lu, X.; McKiernan, M.; Lee, E.P.; Sun, Y.; Xia, Y. Hierarchical nanostructures of K-birnessite nanoplates on anatase nanofibers and their application for decoloration of dye solution. *J. Mater. Chem.* **2010**, *20*, 3157–3162. [CrossRef]
34. Zhuang, X.; Wan, Y.; Feng, C.; Shen, Y.; Zhao, D. Highly efficient adsorption of bulky dye molecules in wastewater on ordered mesoporous carbons. *Chem. Mater.* **2009**, *21*, 706–716. [CrossRef]

35. Bao, N.; Li, Y.; Wei, Z.; Yin, G.; Niu, J. Adsorption of dyes on hierarchical mesoporous TiO_2 fibers and its enhanced photocatalytic properties. *J. Phys. Chem. C* **2011**, *115*, 5708–5719. [CrossRef]
36. Xie, C.; Yang, S.; Shi, J.; Niu, C. Highly crystallized C-doped mesoporous anatase TiO_2 with visible light photocatalytic activity. *Catalysts* **2016**, *6*, 117. [CrossRef]
37. Xu, H.; Li, H.; Xia, J.; Yin, S.; Luo, Z.; Liu, L.; Xu, L. One-pot synthesis of visible-light-driven plasmonic photocatalyst Ag/AgCl in ionic liquid. *ACS Appl. Mater. Interfaces* **2011**, *3*, 22–29. [CrossRef] [PubMed]
38. Ghicov, A.; Yamamoto, M.; Schmuki, P. Lattice Widening in Niobium-Doped TiO_2 Nanotubes: Efficient Ion Intercalation and Swift Electrochromic Contrast. *Angew. Chem. Int. Ed.* **2008**, *47*, 7934–7937. [CrossRef] [PubMed]
39. Qiu, B.; Zhou, Y.; Ma, Y.; Yang, X.; Sheng, W.; Xing, M.; Zhang, J. Facile synthesis of the Ti^{3+} self-doped TiO_2-graphene nanosheet composites with enhanced photocatalysis. *Sci. Rep.* **2015**, *5*, 8591. [CrossRef] [PubMed]
40. Li, K.; Gao, S.; Wang, Q.; Xu, H.; Wang, Z.; Huang, B.; Dai, Y.; Lu, J. In-situ-reduced synthesis of Ti^{3+} self-doped TiO_2/g-C_3N_4 heterojunctions with high photocatalytic performance under led light irradiation. *ACS Appl. Mater. Interfaces* **2015**, *7*, 9023–9030. [CrossRef] [PubMed]
41. Bu, Y.; Chen, Z.; Feng, C.; Li, W. Study of the promotion mechanism of the photocatalytic performance and stability of the Ag@AgCl/g-C_3N_4 composite under visible light. *RSC Adv.* **2014**, *4*, 38124–38132. [CrossRef]
42. Wang, P.; Huang, B.; Qin, X.; Zhang, X.; Dai, Y.; Whangbo, M.-H. Ag/AgBr/$WO_3 \cdot H_2O$: Visible-light photocatalyst for bacteria destruction. *Inorg. Chem.* **2009**, *48*, 10697–10702. [CrossRef] [PubMed]
43. Xu, Y.; Xu, H.; Li, H.; Xia, J.; Liu, C.; Liu, L. Enhanced photocatalytic activity of new photocatalyst Ag/AgCl/ZnO. *J. Alloys Compd.* **2011**, *509*, 3286–3292. [CrossRef]
44. Wang, Z.; Wen, B.; Hao, Q.; Liu, L.-M.; Zhou, C.; Mao, X.; Lang, X.; Yin, W.-J.; Dai, D.; Selloni, A.; et al. Localized excitation of Ti^{3+} ions in the photoabsorption and photocatalytic activity of reduced rutile TiO_2. *J. Am. Chem. Soc.* **2015**, *137*, 9146–9152. [CrossRef] [PubMed]
45. Yin, H.; Wang, X.; Wang, L.; Nie, Q.; Zhang, Y.; Yuan, Q.; Wu, W. Ag/AgCl modified self-doped TiO_2 hollow sphere with enhanced visible light photocatalytic activity. *J. Alloys Compd.* **2016**, *657*, 44–52. [CrossRef]
46. Han, L.; Wang, P.; Zhu, C.; Zhai, Y.; Dong, S. Facile solvothermal synthesis of cube-like Ag@AgCl: A highly efficient visible light photocatalyst. *Nanoscale* **2011**, *3*, 2931–2935. [CrossRef] [PubMed]
47. Ma, B.; Guo, J.; Dai, W.-L.; Fan, K. Highly stable and efficient Ag/AgCl core-shell sphere: Controllable synthesis, characterization, and photocatalytic application. *Appl. Catal. B Environ.* **2013**, *130*, 257–263. [CrossRef]
48. Sung-Suh, H.M.; Choi, J.R.; Hah, H.J.; Koo, S.M.; Bae, Y.C. Comparison of ag deposition effects on the photocatalytic activity of nanoparticulate TiO_2 under visible and UV light irradiation. *J. Photochem. Photobiol. A Chem.* **2004**, *163*, 37–44. [CrossRef]
49. Yu, J.-G.; Yu, H.-G.; Cheng, B.; Zhao, X.-J.; Yu, J.C.; Ho, W.-K. The effect of calcination temperature on the surface microstructure and photocatalytic activity of TiO_2 thin films prepared by liquid phase deposition. *J. Phys. Chem. B* **2003**, *107*, 13871–13879. [CrossRef]
50. Cheng, H.; Huang, B.; Dai, Y.; Qin, X.; Zhang, X. One-step synthesis of the nanostructured AgI/BiOI composites with highly enhanced visible-light photocatalytic performances. *Langmuir* **2010**, *26*, 6618–6624. [CrossRef] [PubMed]
51. Klaysri, R.; Tubchareon, T.; Praserthdam, P. One-step synthesis of amine-functionalized TiO_2 surface for photocatalytic decolorization under visible light irradiation. *J. Ind. Eng. Chem.* **2017**, *45*, 229–236. [CrossRef]
52. Zhu, M.; Chen, P.; Liu, M. Ag/Agbr/graphene oxide nanocomposite synthesized via oil/water and water/oil microemulsions: A comparison of sunlight energized plasmonic photocatalytic activity. *Langmuir* **2012**, *28*, 3385–3390. [CrossRef] [PubMed]
53. Sun, L.; Zhang, R.; Wang, Y.; Chen, W. Plasmonic Ag@AgCl nanotubes fabricated from copper nanowires as high-performance visible light photocatalyst. *ACS Appl. Mater. Interfaces* **2014**, *6*, 14819–14826. [CrossRef] [PubMed]
54. Bao, N.; Li, Y.; Yu, X.-H.; Niu, J.-J.; Wu, G.-L.; Xu, X.-H. Removal of anionic azo dye from aqueous solution via an adsorption–photosensitized regeneration process on a TiO_2 surface. *Environ. Sci. Pollut. Res.* **2013**, *20*, 897–906. [CrossRef] [PubMed]

55. Ye, L.; Liu, J.; Gong, C.; Tian, L.; Peng, T.; Zan, L. Two different roles of metallic Ag on Ag/AgX/BiOX (X = Cl, Br) visible light photocatalysts: Surface plasmon resonance and Z-scheme bridge. *ACS Catal.* **2012**, *2*, 1677–1683. [CrossRef]
56. Hirakawa, T.; Kamat, P.V. Charge separation and catalytic activity of $Ag@TiO_2$ core-shell composite clusters under UV-irradiation. *J. Am. Chem. Soc.* **2005**, *127*, 3928–3934. [CrossRef] [PubMed]
57. Zhang, Q.; Bao, N.; Wang, X.; Hu, X.; Miao, X.; Chaker, M.; Ma, D. Advanced fabrication of chemically bonded graphene/TiO_2 continuous fibers with enhanced broadband photocatalytic properties and involved mechanisms exploration. *Sci. Rep.* **2016**, *6*, 38066. [CrossRef] [PubMed]